transcatheter hepatic arterial embolization. *Cancer* 1986;57:1184–91.
27. Kenji J, Hyodo I, Tanimizu M, Tanada M, Nishikawa Y, Hosokawa Y, Mandai K, Moriwaki S. Total necrosis of hepatocellular carcinoma with a combination therapy of arterial infusion of chemotherapeutic lipiodol and transcatheter arterial embolization: report of 14 cases. *Semin Oncol* 1997;24: S6–71–S6–80.
28. Kobayashi N, Ishii M, Ueno Y, Kisara N, Chida N, Iwasaki T, Toyota T. Co-expression of Bcl-2 protein and vascular endothelial growth factor in hepatocellular carcinomas treated by chemoembolization. *Liver* 1999;19:25–31.
29. Xiao EH, Li JQ, Huang JF. Effects of p53 on apoptosis and proliferation of hepatocellular carcinoma cells treated with transcatheter arterial chemoembolization. *World J Gastroenterol* 2004;10:190–4.
30. Kanai M, Kohda H, Sekiya C, Namiki M. Effects on interleukin 1 alpha and beta production of peripheral blood mononuclear cells from patients with hepatocellular carcinoma after transcatheter arterial embolization. *Gastroenterol Jpn* 1990;25:662.
31. Yamazaki H, Nishimoto N, Oi H, Matsushita M, Ogata A, Shima Y, Inoue T, Tang JT, Yoshizaki K, Kishimoto T, Inoue T. Serum interleukin 6 as a predicator of the therapeutic effect and adverse reactions after transcatheter arterial embolization. *Cytokine* 1995;7:191–5.
32. Itoh Y, Okanoue T, Ohnishi N, Nishioji K, Sakamoto S, Nagao Y, Nakamura H, Kirishima T, Kashima K. Hepatic damage induced by transcatheter arterial chemoembolization elevates serum concentrations of macrophage-colony stimulating factor. *Liver* 1999;19:97–103.
33. Araki T, Itai Y, Furui S, Tasaka A. Dynamic CT densitometry of hepatic tumors. *AJR Am J Roentgenol* 1980;135: 1037–43.
34. Sobin LH, Wittekind C. TNM classification of malignant tumors, 6th edn. New York: Wiley-Liss, 2002. 81.
35. Terayama N, Miyayama S, Tatsu H, Yamamoto T, Toya D, Tanaka N, Mitsui T, Miura S, Fujisawa M, Kifune K, Matsui O, Takashima T. Subsegmental transcatheter arterial embolization for hepatocellular carcinoma in the caudate lobe. *J Vasc Interv Radiol* 1998;9:501–8.
36. Okamoto H, Shin J, Mion S, Koshimura S, Shimizu R. Studies on the anticancer and streptolysin S-forming abilities of hemolytic streptococci. *Jpn J Microbiol* 1967;11: 323–36.
37. Nakahara S, Tsunoda T, Baba T, Asabe S, Tahara H. Dendritic cells stimulated with a bacterial product, OK-432, efficiently induce cytotoxic T lymphocytes specific to tumor rejection peptide. *Cancer Res* 2003; 63:4112–8.
38. Japan LCSGo. Classification of primary liver cancer. English edn. 2. Tokyo: Kanehara, 1997.
39. Desmet VJ, Gerber M, Hoofnagle JH, Manns M, Scheuer PJ. Classification of chronic hepatitis: diagnosis, grading and staging. *Hepatology* 1994;19:1513–20.
40. Mizukoshi E, Nakamoto Y, Marukawa Y, Arai K, Yamashita T, Tsuji H, Kuzushima K, Takiguchi M, Kaneko S. Cytotoxic T cell responses to human telomerase reverse transcriptase in patients with hepatocellular carcinoma. *Hepatology* 2006;43:1284–94.
41. Mizukoshi E, Honda M, Arai K, Yamashita T, Nakamoto Y, Kaneko S. Expression of multidrug resistance-associated protein 3 and cytotoxic T cell responses in patients with hepatocellular carcinoma. *J Hepatol* 2008;49:946–54.
42. Ikeda-Moore Y, Tomiyama H, Miwa K, Oka S, Iwamoto A, Kaneko Y, Takiguchi M. Identification and characterization of multiple HLA-A24-restricted HIV-1 CTL epitopes: strong epitopes are derived from V regions of HIV-1. *J Immunol* 1997;159: 6242–52.
43. Kuzushima K, Hayashi N, Kimura H, Tsurumi T. Efficient identification of HLA-A*2402-restricted cytomegalovirus-specific CD8(+) T-cell epitopes by a computer algorithm and an enzyme-linked immunospot assay. *Blood* 2001;98:1872–81.
44. Wissniowski TT, Hansler J, Neureiter D, Frieser M, Schaber S, Esslinger B, Voll R, Strobel D, Hahn EG, Schuppan D. Activation of tumor-specific T lymphocytes by radio-frequency ablation of the VX2 hepatoma in rabbits. *Cancer Res* 2003;63: 6496–500.
45. Korbelik M, Krosl G, Krosl J, Dougherty GJ. The role of host lymphoid populations in the response of mouse EMT6 tumor to photodynamic therapy. *Cancer Res* 1996;56: 5647–52.
46. Udagawa M, Kudo-Saito C, Hasegawa G, Yano K, Yamamoto A, Yaguchi M, Toda M, Azuma I, Iwai T, Kawakami Y. Enhancement of immunologic tumor regression by intratumoral administration of dendritic cells in combination with cryoablative tumor pretreatment and Bacillus Calmette-Guerin cell wall skeleton stimulation. *Clin Cancer Res* 2006;12: 7465–75.
47. Machlenkin A, Goldberger O, Tirosh B, Paz A, Volovitz I, Bar-Haim E, Lee SH, Vadai E, Tzehoval E, Eisenbach L. Combined dendritic cell cryotherapy of tumor induces systemic antimetastatic immunity. *Clin Cancer Res* 2005;11: 4955–61.
48. Ladhams A, Schmidt C, Sing G, Butterworth L, Fielding G, Tesar P, Strong R, Leggett B, Powell L, Maddern G, Ellem K, Cooksley G. Treatment of non-resectable hepatocellular carcinoma with autologous tumor-pulsed dendritic cells. *J Gastroenterol Hepatol* 2002;17: 889–96.
49. Iwashita Y, Tahara K, Goto S, Sasaki A, Kai S, Seike M, Chen CL, Kawano K, Kitano S. A phase I study of autologous dendritic cell-based immunotherapy for patients with unresectable primary liver cancer. *Cancer Immunol Immunother* 2003; 52:155–61.
50. Lee WC, Wang HC, Hung CF, Huang PF, Lia CR, Chen MF. Vaccination of advanced hepatocellular carcinoma patients with tumor lysate-pulsed dendritic cells: a clinical trial. *J Immunother* 2005;28: 496–504.
51. Lee JS, Thorgeirsson SS. Genome-scale profiling of gene expression in hepatocellular carcinoma: classification, survival prediction, and identification of therapeutic targets. *Gastroenterology* 2004; 127:S51–5.
52. Thimme R, Neagu M, Boettler T, Neumann-Haefelin C, Kersting N, Geissler M, Makowiec F, Obermaier R, Hopt UT, Blum HE, Spangenberg HC. Comprehensive analysis of the alpha-fetoprotein-specific CD8+ T cell responses in patients with hepatocellular carcinoma. *Hepatology* 2008;48:1821–33.

Crucial Contribution of Thymic Sirpα^+ Conventional Dendritic Cells to Central Tolerance against Blood-Borne Antigens in a CCR2-Dependent Manner

Tomohisa Baba,* Yasunari Nakamoto,† and Naofumi Mukaida[1]*

Thymic dendritic cells (DCs) as well as thymic epithelial cells are presumed to be major sentinels in central tolerance by inducing the apoptosis of autoreactive T progenitor cells. The thymic DC population is composed of heterogeneous subsets including CD11c$^+$B220$^+$ plasmacytoid DCs, CD11c$^+$B220$^-$CD8α^+ signal regulatory protein α (Sirpα)$^-$ and CD11c$^+$B220$^-$CD8α^-Sirpα^+ conventional DCs (cDCs). However, the distinctive role of each DC subset remains undefined. We show herein that Sirpα^+ cDCs, a minor subpopulation, was disseminated in the thymic cortical area with some of them uniquely localized inside perivascular regions and nearby small vessels in the thymus. The Sirpα^+ but not Sirpα^- cDC subset can selectively capture blood-circulating Ags. Moreover, in CCR2-deficient mice, the thymic Sirpα^+ cDC subset, but not other thymic cell components, was moderately decreased especially in the perivascular regions. Concomitantly, these mice exhibited a modest impairment in intrathymic negative selection against blood-borne Ags, with the reduced capacity to uptake blood-borne Ags. Given their intrathymic cortical localization, CD11c$^+$B220$^-$CD8α^-Sirpα^+ cDCs can have a unique role in the development of central tolerance against circulating peripheral Ags, at least partially in a CCR2-dependent manner. *The Journal of Immunology,* **2009, 183: 3053–3063.**

The thymus is vital for development of T cells. T progenitor cells in the thymus are subjected to positive and negative selection, and survivors become self-MHC-restricted and self-tolerant mature naive T cells. Negative selection induces clonal deletion of potentially pathogenic autoreactive T cells and consequently decreases the risk of the development of autoimmune disorders (1). Thus, negative selection has a major role in central tolerance. Medullary thymic epithelial cells (mTECs)[2] are major inducers of negative selection. mTECs express the *autoimmune regulator (AIRE)* gene, which induces the ectopic expression of a milieu of peripheral tissue-specific Ags in the thymus resulting in the clonal deletion of autoreactive T progenitors with specificity for these Ags (2–4). Another type of thymic APCs, in particularly dendritic cells (DCs), have also been shown to contribute to negative selection (5–7). However, the detailed molecular and cellular mechanisms by which thymic DCs mediate negative selection remain largely unknown.

Thymic DCs are heterogeneous, similar to DCs in peripheral lymphoid organs such as lymph nodes and spleen. In humans and mice, thymic DCs are classified into two distinct subsets, CD11c$^+$B220$^+$ plasmacytoid DCs (pDCs) and CD11c$^+$B220$^-$ conventional DCs (cDCs). cDCs are further divided into CD11c$^+$CD11b$^-$CD8α^+Sirpα^- and CD11c$^+$CD11b$^+$CD8α^-Sirpα^+ subsets (8, 9). CD8α^+Sirpα^- cDCs, the most abundant subset among these three thymic DC subsets, are clustered in the medulla (10, 11). These CD8α^+Sirpα^- cDCs also express AIRE and can present endogenous self-Ags. In addition, they can cross-present tissue-specific Ags derived from the mTECs for negative selection (12, 13). In contrast, the intrathymic location and functions of another minor cDC, CD11c$^+$CD11b$^+$CD8α^-Sirpα^+, subset remain unclear, although this subset is presumed to migrate from the bloodstream (8). Proietto et al. (14) demonstrated that Sirpα^+ cDCs can induce thymocytes to efficiently differentiate into regulatory T cells in vitro. However, the roles of Sirpα^+ cDCs in central tolerance and regulatory T cell generation in vivo and the nature of the target autoantigens of central tolerance remain elusive.

Chemokines and their receptors have essential roles in controlling the homeostatic homing of immune cells including DCs and T cells (15–17). We examined the composition of thymic DC subsets in mice deficient in CCR1, CCR2, CCR5, or CX3CR1, the chemokine receptors which are expressed by DCs (18, 19). We observed that Sirpα^+ cDCs, but not Sirpα^- cDCs or pDCs, were selectively decreased in the thymus of CCR2-deficient mice, but not in the other chemokine receptor gene-deficient mice. Interestingly, CCR2-deficient mice exhibited a modest impairment in intrathymic negative selection against i.v. injected Ags. Concomitantly, CCR2 deficiency allowed releasing more autoreactive T cells against serum Ags into periphery. These Sirpα^+ cDCs migrated from bone marrow to thymus by the way of the peripheral blood and showed a unique intrathymic localization confined to perivascular and cortical areas. Moreover, Sirpα^+ cDCs had a greater capacity to uptake blood-borne Ags than Sirpα^- cDCs, along with their unique intrathymic localization. Thus, our present study suggests that thymic Sirpα^+ cDCs may function as a specialized APC for the development of central tolerance to blood-borne Ags.

*Division of Molecular Bioregulation, Cancer Research Institute and †Department of Disease Control and Homeostasis, Graduate School of Medical Science, Kanazawa University, Kanazawa, Ishikawa, Japan

Received for publication February 13, 2009. Accepted for publication June 8, 2009.

The costs of publication of this article were defrayed in part by the payment of page charges. This article must therefore be hereby marked *advertisement* in accordance with 18 U.S.C. Section 1734 solely to indicate this fact.

[1] Address correspondence and reprint requests to Dr. Naofumi Mukaida, Division of Molecular Bioregulation, Cancer Research Institute, Kanazawa University, 13-1 Takara-machi, Kanazawa 920-0934, Japan. E-mail address: naofumim@kenroku.kanazawa-u.ac.jp

[2] Abbreviations used in this paper: mTEC, medullary thymic epithelial cell; DC, dendritic cell; Sirpα, signal regulatory protein α; pDC, plasmacytoid DC; cDC, conventional DC; WT, wild type; Col IV, type IV collagen; FCM, flow cytometry; CMFDA, 5-chloromethylfluorescien diacetate; Cyt D, cytochalasin D; FSC, forward scatter; SSC, side scatter; DP, double positive.

www.jimmunol.org/cgi/doi/10.4049/jimmunol.0900438

Materials and Methods

Mice

Specific pathogen-free 6- to 7-wk-old male BALB/c mice were purchased from Charles River Japan and designated as wild-type (WT) mice. CCR1$^{-/-}$ and CX3CR1$^{-/-}$ mice were provided by Dr. P. M. Murphy (National Institute of Allergy and Infectious Diseases, National Institutes of Health, Bethesda, MD) (20, 21). CCR2$^{-/-}$ (22) and CCR5$^{-/-}$ mice (23) were provided by Dr. W. Kuziel (University of Texas San Antonio, San Antonio, TX) and Dr. Kouji Matsushima (University of Tokyo, Tokyo, Japan), respectively. All chemokine receptor-deficient mice were backcrossed to BALB/c mice for 8–10 generations. DO11.10 mice expressing a transgenic TCR that recognizes the $OVA_{323-339}$ peptide in the context of I-A^d were maintained as heterozygotes. DO11.10 mice were backcrossed to CCR2$^{-/-}$ mice to generate DO11.10/CCR2$^{-/-}$ mice. Genotyping for the *CCR2* gene was done by direct PCR from whole blood samples using an Ampdirect Plus kit (Shimadzu) and the specific primers (sense, 5′-CACGAAGTATCCAAGAGCTTG-3′ and antisense, 5′-CCCAAGTGAC TACACTTGTTA-3′). The mouse experiments were performed under specific pathogen-free conditions in accordance with the Guidelines for the Care and Use of Laboratory Animals of Kanazawa University.

Antibodies

Rat anti-mouse mAbs used were anti-CD3ε (145-2C11; Miltenyi Biotec), anti-CD4 (RM4-5; BD Pharmingen), anti-CD8 (53-6.7; BD Pharmingen), anti-CD25 (PC61; BD Pharmingen), anti-CD45R/B220 (RA3-6B2; BD Pharmingen), anti-CD172a/Sirpα (P84; BD Pharmingen), anti-DO11.10 clonotypic TCR (KJ1-26; BD Pharmingen), anti-F4/80 (A3-1; Serotec), and anti-Ly51 (6C3; BioLegend). Hamster anti-mouse CD11c (HL-3) and mouse anti-mouse I-A^d (AMS-32.1) mAbs were purchased from BD Pharmingen. Rabbit anti-mouse CCR2 mAb and anti-mouse type IV collagen (Col IV) polyclonal Ab were purchased from Epitomics and LSL, respectively. Goat anti-mouse MCP-2 polyclonal Ab was purchased from Santa Cruz Biotechnology. Isotype-matched control IgGs for each rat and hamster mAbs were purchased from BD Pharmingen. Mouse, rabbit, and goat IgG (Sigma-Aldrich) served as controls.

Cell preparation

Thymus was digested in 0.6 mg/ml collagenase type IV (Sigma-Aldrich) and 25 Kunitz units/ml DNase I (Sigma-Aldrich) in RPMI 1640 (Sigma-Aldrich) at 37°C for 20 min. The low-density cells were further isolated from the resultant single-cell suspensions using Histopaque-1077 reagent (Sigma-Aldrich). PBMCs were isolated from whole blood using Histopaque-1083 reagent (Sigma-Aldrich). Bone marrow cells were washed out with cold RPMI 1640 medium from the femoral and tibial bones.

Flow cytometry (FCM)

The low-density cells from thymus, PBMCs, and bone marrow cells were stained with various combinations of fluorescent dye-conjugated or nonconjugated specific Abs in PBS supplemented with 2 mM EDTA and 3% FBS. For nonconjugated Abs, fluorescent-conjugated secondary Abs were used. After washing in PBS, expression of cell surface molecular markers was analyzed using a FACSCalibur (BD Biosciences) with CellQuest Pro software (BD Biosciences).

Histology and fluorescent immunohistochemistry

Thymic tissues were frozen in OCT compound (Sakura) and 6-μm-thick cryostat sections were stained with H&E. For immunofluorescence analysis, 6-μm-thick cryostat sections were fixed with cold acetone for 3 min and incubated with Protein Block Reagent (DakoCytomation) to block nonspecific binding. Then fluorescent immunostaining was done by the standard method (for details, see the figure legends). After washing with 0.05% Tween 20-PBS, slides were mounted in fluorescent mounting medium (DakoCytomation). Immunofluorescence was detected in a setting that excluded the nonspecific signal of the isotype control using a fluorescence microscope (BX50; Olympus) or confocal laser-scanning microscope (LSM510; Zeiss). DP Controller software (Olympus) and Zen 2007 software (Zeiss) were used for image processing.

RT-PCR

Total RNAs were extracted from tissues using a RNeasy Mini Kit (Qiagen) and then reverse-transcribed using SuperScript III First-Strand Synthesis System (Invitrogen). PCR was done using the cDNAs, 2.5 mM dNTP mix (Takara), TaqDNA polymerase (Takara), and the specific primer sets for the *GAPDH* gene (sense, 5′-CAC TGA GCA TCT CCC TCA CA-3′ and antisense, 5′-TGG GTG CAG CGA ACT TTA TT-3′), *CD45* gene (sense, 5′-AAG ACA GAG TGC AAA GGA GAC-3′ and antisense, 5′-TGT AGG TGT TTG CCC TGT GAC AAA GAC-3′), *keratin 8* gene (sense, 5′-ACG GTG AAC CAG AGC CTG T-3′ and antisense, 5′-CTC CAC TTG GTC TCC AGC AT-3′), *MCP-1* gene (sense, 5′-CCC ACT CAC CTG CTG CTA CT-3′ and antisense, 5′-TCT GGA CCC ATT CCT TCT TG-3′), *MCP-2* gene (sense, 5′-CAG TCA CCT GCT GCT TTC AT-3′ and antisense, 5′-ATA CCC TGC TTG GTC TGG AA-3′), and *MCP-3* gene (sense, 5′-AAA CAA AAG ATC CCC AAG AGG-3′ and antisense, 5′-CAC AGA CTT CCA TGC CCT TC-3′) for 30 cycles of 95°C for 30 s, 55°C for 30 s, and 72°C for 30 s.

Effects of a peptide Ag on DO11.10 clonotypic thymocytes

DO11.10-transgenic mice with or without *CCR2* gene deficiency were administered 200 μg of $OVA_{323-339}$ peptide (ABGENT) in PBS through the tail vein. To induce thymocyte deletion independently of Ag presentation, mice were injected i.p. with 50 μg of anti-CD3ε mAb (24). Two days after injection, thymocytes were collected and stained with the following combinations of Abs: anti-CD4, anti-CD8, and anti-DO11.10 or anti-CD4, anti-CD25, and anti-DO11.10 Abs. To detect apoptotic cells, thymocytes were stained using an Annexin V-FITC Apoptosis Detection Kit (Merck). After being stained, the cells were analyzed by FCM.

Trafficking of bone marrow-derived immature DCs injected into bone marrow

Bone marrow cells were cultured in RPMI 1640 medium supplemented with 10% FBS and mouse GM-CSF (R&D Systems) at a concentration of 20 ng/ml. An equal volume of culture medium of the same content was added at 4 days, and one-half of the medium was replaced with fresh culture medium at 7 days after the plating. Most bone marrow cells were differentiated into immature DCs as judged by morphological appearances at 10 days after the initiation of the culture. The resultant immature DCs were stained with 1 μM 5-chloromethylfluorescein diacetate (CMFDA; Invitrogen) dye and 1 million cells were injected into the tibial bone marrow cavity of each mouse. After the injection, low-density cells were obtained from thymus, lymph nodes, or PBMCs to determine the presence of CMFDA-stained DCs by using FCM.

Localization of the i.v. injected Ags

Alexa Fluor 488-conjugated OVA protein (OVA_{488}), Alexa Fluor 647-conjugated OVA protein (OVA_{647}) (Invitrogen), or mouse serum IgG (Sigma-Aldrich), which was conjugated with Alexa Fluor 647, using an Alexa Fluor 647 protein labeling kit (Invitrogen), was injected into the tail vein of mice. Thymic low-density cells and PBMCs were isolated at the indicated time points after OVA protein injection and were stained with anti-CD11c and anti-Sirpα Abs. Then the cells were analyzed by FCM. For the localization of the Ag uptake, cryostat sections of frozen thymic tissues were obtained from mice injected with OVA protein and were stained with anti-Sirpα, anti-CD11c, anti-I-A^d, anti-Ly51, or anti-Col IV Abs and were then observed by fluorescence microscope.

In vitro endocytosis assay

Low-density cells were isolated from the thymus and were incubated with 10 μg/ml OVA_{647} in RPMI 1640 at 37°C for 20 min. As a negative control, incubation was conducted on ice. Endocytosis by each thymic DC subset was analyzed by FCM after being stained with anti-CD11c and anti-Sirpα Abs. In some experiments, low-density cells were preincubated with 10 μM cytochalasin D (Cyt D; Sigma-Aldrich), an actin inhibitor (25), 100 mM ammonium chloride (NH_4Cl) (Wako), an inhibitor of the clathrin-dependent pathway (26), or 0.5 mg/ml mannan (Sigma-Aldrich) at 37°C for 15 min before incubation with OVA_{647} at 37°C for 20 min in the presence of fresh inhibitors.

Adoptive transfer of bone marrow cells

Bone marrow cells were obtained from WT or CCR2$^{-/-}$ mice and were stained with 2 μM CMFDA dye. Twenty million cells were injected into the tail vein of CCR2$^{-/-}$ mice. OVA_{647} was injected into the tail vein at 2 days after injection. Thymic low-density cells were isolated at 1 h after OVA protein injection, and the presence of donor-derived Sirpα$^+$ cDCs and their capability of Ag uptake were analyzed by FCM.

In vivo cell proliferation assay

Spleen mononuclear cells were isolated from WT or CCR2$^{-/-}$ mice and were labeled with 25 μM CFSE using a CellTrace CFSE Cell Proliferation Kit (Invitrogen). Ten million prelabeled cells were injected into the tail vein of WT mice. One day after injection, mice were immunized with total

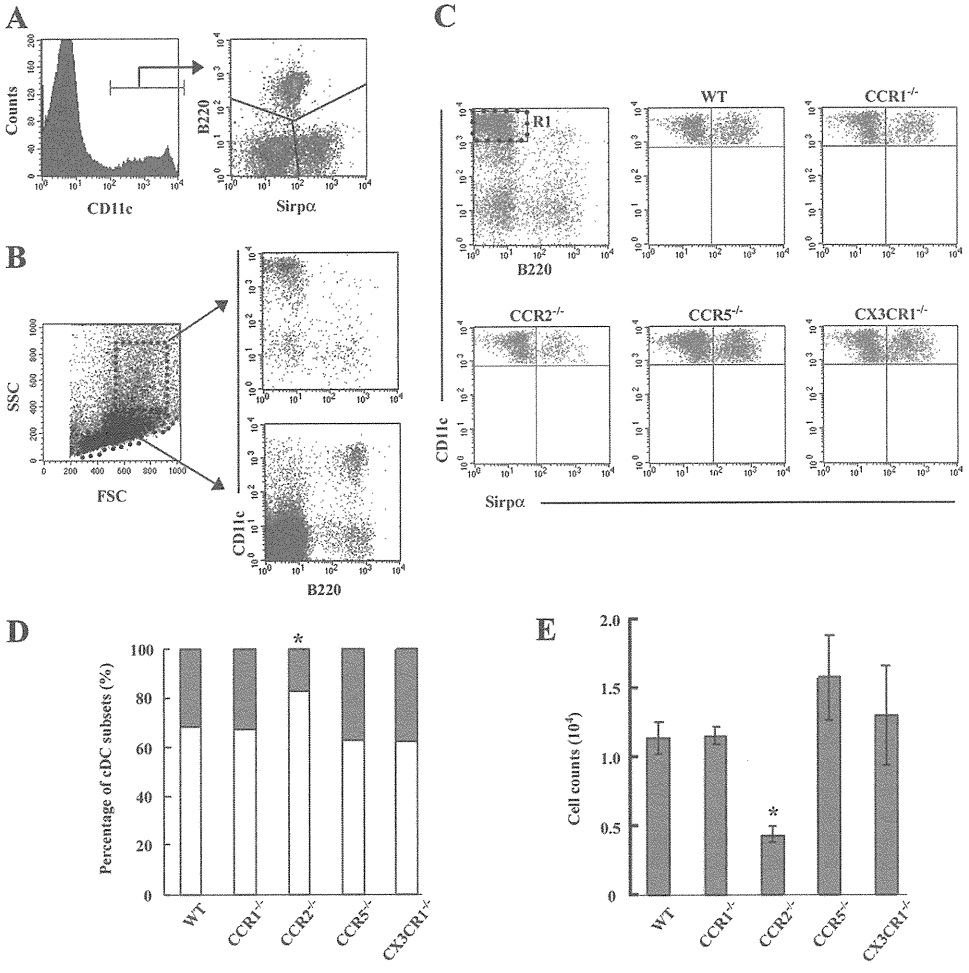

FIGURE 1. Effects of chemokine receptor deficiency on mouse thymic DC subsets. *A*, Low-density cells were isolated from WT mouse thymus and were stained with PE-conjugated anti-CD11c, allophycocyanin-conjugated anti-B220, and nonconjugated anti-Sirpα mAbs, followed by staining with FITC-conjugated mouse anti-rat IgG1. The $CD11c^+$ DC populations were gated to analyze the expression of Sirpα and B220. *B*, Thymic low-density cells were divided into two groups based on their FSC and SSC patterns, which are indicated by elliptic and square gates. Then DC subsets in each region were analyzed. *C*, Low-density cells were isolated from WT, $CCR1^{-/-}$, $CCR2^{-/-}$, $CCR5^{-/-}$, and $CX3CR1^{-/-}$ mice. The $Sirp\alpha^-$ and $Sirp\alpha^+$ subsets in FSC^{high} $SSC^{high}CD11c^{high}B220^-$ cDC populations gated with region 1 (R1) were compared among these mice. *D*, The ratio of two DC subsets (blank portion, $Sirp\alpha^-$ subset; gray portion, $Sirp\alpha^+$ subset) present in thymic cDC population was determined. Data represent the mean of three independent experiments. *E*, The numbers of $Sirp\alpha^+$ DCs in the thymus. Data represent mean ± SD from three independent experiments. *, $p < 0.01$.

mouse serum protein emulsified in CFA. PBS in CFA was immunized as a control. Two days after immunization, lymphocytes were harvested from draining and nondraining lymph nodes and stained with anti-CD4 mAb. The percentage of CFSE-diluted divided cells was analyzed by FCM.

Statistical analysis

Data are represented as mean ± SD. Statistical significance was determined by one-way ANOVA followed by the Tukey-Kramer test. A value of $p < 0.05$ was considered statistically significant.

Results

Selective reduction of thymic $Sirp\alpha^+$ cDCs in $CCR2^{-/-}$ mice

Consistent with a previous report (8), three distinct populations of thymic $CD11c^+$ DCs have been identified: $B220^+$ pDC, $B220^-$ $Sirp\alpha^-$ cDC, and $B220^-Sirp\alpha^+$ cDC subsets (Fig. 1*A*). cDC and pDC subsets were present mainly in the forward scatter (FSC^{high}), side scatter SSC^{high}, and SSC^{low} areas upon FCM, respectively (Fig. 1*B*). The pivotal role of chemokines in the trafficking of DCs prompted us to examine thymic DC subsets in mice deficient in chemokine receptor genes. $Sirp\alpha^+$ DCs were markedly decreased in $CCR2^{-/-}$ mice, compared with WT mice, both in the relative (Fig. 1, *C* and *D*) and absolute number (Fig. 1*E*), whereas $Sirp\alpha^-$ DC (Fig. 1*C*) and $B220^+$ pDC numbers (data not shown) were not changed in $CCR2^{-/-}$ mice. In contrast, no significant changes were observed on thymic cDC and pDC subsets in mice deficient in other chemokine receptors including CCR1, CCR5, and CX3CR1. Moreover, we did not observe any differences in thymic $B220^+$ B cell and $F4/80^+$ macrophage numbers between WT and $CCR2^{-/-}$ mice (data not shown). Microscopic studies of the thymus failed to reveal any morphological differences between WT and $CCR2^{-/-}$ mice in terms of the total cellularity, the distribution of thymocytes in each developmental stage, and the localization of $Ly51^+$ cortical thymic epithelial cells and $I\text{-}A^{d\ high}$ mTEC (supplemental Fig. S1[3]). Thus, $CCR2^{-/-}$ mice exhibit a selective decrease in the $Sirp\alpha^+$ DC subset in thymus.

Attenuation of $OVA_{323–339}$ peptide-induced clonal deletion by CCR2 gene ablation

$Sirp\alpha^+$ DCs are presumed to have the capacity to carry peripheral tissue Ags into the thymus (14). We next investigated the roles of $Sirp\alpha^+$ DCs in thymus on taking in an i.v. administered Ag. PBS injection did not cause any changes in each developmental stage of thymocytes in DO11.10 and DO11.10/$CCR2^{-/-}$ mice (data not shown). On the contrary, i.v. administration of $OVA_{323–339}$ peptide markedly reduced the proportion and absolute number of clonotypic CD4/CD8 double-positive (DP) thymocytes in DO11.10 mice. *CCR2* gene ablation modestly attenuated this reduction (Fig. 2, *A–C*). OVA peptide injection consistently increased the proportion of annexin V^+ apoptotic cells in DO11.10 mouse thymus compared with that in DO11.10/$CCR2^{-/-}$ mice (Fig. 2*D*). In contrast, OVA peptide induced a modest increase in the number of $DO11.10^+CD25^+CD4^+$ regulatory T cell phenotype to similar extents in both DO11.10 and DO11.10/$CCR2^{-/-}$ thymus (Fig. 2*E*). Thus, decreased thymic $Sirp\alpha^+$ DCs in $CCR2^{-/-}$ mice may be associated with a moderately impaired thymic negative selection. Moreover, following i.p. injection with anti-CD3 Ab (24), thymocytes were deleted to similar extents in DO11.10 and DO11.10/$CCR2^{-/-}$ mice

[3] The online version of this article contains supplemental material.

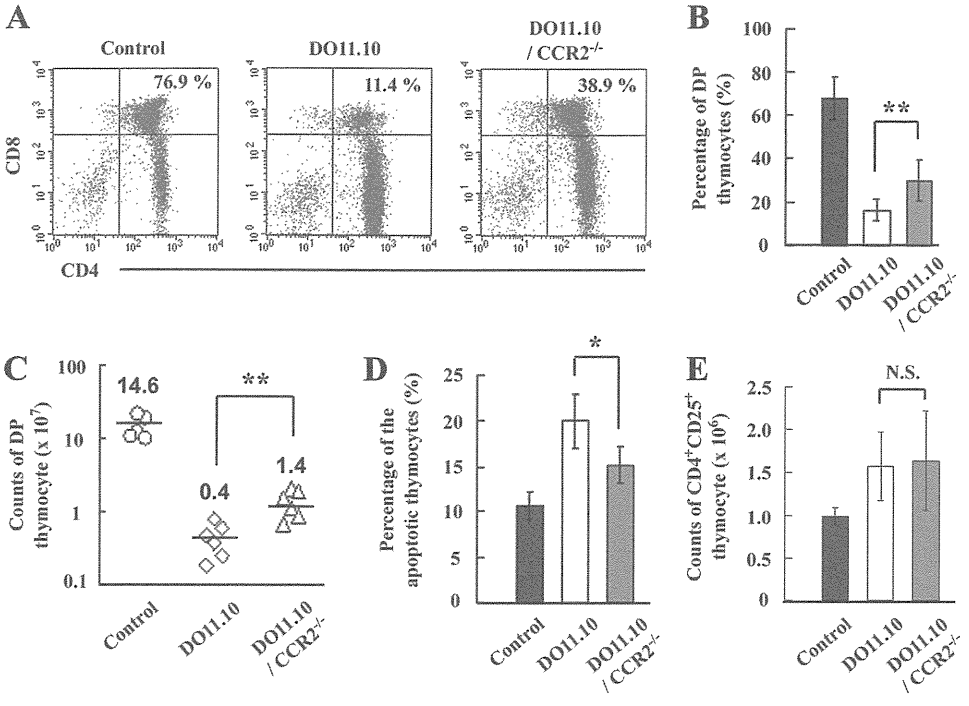

FIGURE 2. Induction of clonal deletion of DO11.10 clonotypic thymocytes. To induce the clonal deletion, 200 μg of $OVA_{323-339}$ peptide in PBS was injected into the tail vein of DO11.10-transgenic or DO11.10/$CCR2^{-/-}$ mice. PBS was injected as a control. DO11.10-transgenic TCR-expressing thymocytes were identified as KJ1-26-positive cells. *A*, Each developmental stage of thymocytes after $OVA_{323-339}$ peptide injection. Percentage of DP stage is shown in each panel. *B*, Percentage of DP stage of development; *C*, the number of DP thymocytes; *D*, percentage of the apoptotic thymocytes; and *E*, the number of $CD4^+$ $CD25^+$ thymocytes were determined on DO11.10 and DO11.10/$CCR2^{-/-}$ mice. Representative results from at least four independent experiments are shown in *A* while the mean ± SD was calculated on at least four independent experiments and are shown in *B–E*. *, $p < 0.05$ and **, $p < 0.01$. N.S., No significant difference.

(supplemental Fig. S2), indicating the absence of intrinsic defects of thymocytes in the absence of CCR2. These results collectively suggest that thymic Sirpα^+ DCs can contribute to intrathymic negative selection of a bloodstream-derived Ag without inducing regulatory T cells.

Thymic Sirpα^+ DCs can efficiently capture peripheral Ag from bloodstream

To elucidate the functions of thymic Sirpα^+ DCs more in detail, we determined their intrathymic localization. In thymi of WT mice, Sirpα was mainly detected on $CD11c^+$ DCs scattered in the thymic cortex (Fig. 3, *A* and *B*), but not on $CD11c^+$ DCs clustered in medulla, the predominating site of thymic $CD8\alpha^+$Sirpα^- DCs. Moreover, most Sirpα^+ DCs were localized in close proximity to small vessels with single Col IV^+ basement membrane or inside perivascular regions (PVRs) separated by two Col IV^+ basement membranes in the cortex (Fig. 3*C*). The thymic DC population includes APCs crucially involved in the central tolerance system involving bloodstream C5 Ag (27). Furthermore, Sirpα^+ DCs are selectively localized in PVRs or in close proximity to small vessels, both essential components of the blood-thymus barrier (28). Hence, we hypothesized that this DC subset might be involved in Ag uptake from the bloodstream. To address this possibility, we treated WT mice i.v. with OVA_{647} and examined its uptake by thymic DCs. Intrathymic Sirpα^+ DCs, but not Sirpα^- DCs, took up OVA protein in a dose-dependent manner (Fig. 4*A*), maintaining a stable level from 1 to 4 h after the injection and decreasing thereafter (Fig. 4*B*). Recently, it was reported that bloodstream DCs could efficiently capture and transport particulate bacteria into the spleen when particulate bacteria were i.v. injected (29). Indeed, bloodstream $CD11c^+$ cells rapidly disappeared from the peripheral blood after capturing OVA protein (Fig. 4*C*). By contrast, the uptake by intrathymic Sirpα^+ DCs reached a peak level at 15 min, decreasing to the stable level thereafter. Thus, there may be a remote possibility that circulating DCs migrated into the thymus after capturing OVA protein inside the bloodstream. Furthermore, in addition to an exogenous protein, intrathymic Sirpα^+ DCs also captured an endogenous serum protein, mouse IgG, which was conjugated with Alexa Fluor 647, when it was administered i.v. (supplemental Fig. S3). Thus, Sirpα^+ DCs can effectively capture peripheral Ags from the bloodstream across the blood-thymus barrier. This notion was further supported by the observation that Sirpα^+ DCs engulfed OVA protein with a higher efficiency than Sirpα^- DCs when cultured in vitro with OVA_{647} (Fig. 4, *D* and *E*). Mannan from *Saccharomyces cerevisiae*, but not NH_4Cl or Cyt D from *Zygosporium mansonii*, markedly inhibited endocytosis of OVA protein by Sirpα^- DCs (Fig. 4*F*, *upper panel*). On the contrary, uptake of OVA protein by Sirpα^+ DCs was markedly attenuated by NH_4Cl and Cyt D, but not mannan (Fig. 4*F*, *lower panel*). These observations suggest that thymic Sirpα^+ DCs can endocytose soluble Ags more efficiently than Sirpα^- DCs, in a clathrin-dependent, but not mannose receptor-dependent manner.

Thymic Sirpα^+ DCs capture peripheral Ag inside PVRs or nearby small vessels, and then migrate into the cortical parenchyma

We examined sequentially intrathymic localization of OVA-derived signals after i.v. injection of OVA_{488}. By 0.5 h, OVA_{488}-derived signals were detected in Sirpα^+ cells (Fig. 5*A*), $CD11c^+$ DCs (Fig. 5*B*) and inside PVRs or in close proximity to small vessels (Fig. 5*C*). Although some signals remained nearby in small vessels, signals inside PVRs were obviously decreased at 6 h (Fig. 5*D*), as judged by the Col IV immunostaining pattern. At 18 h after the injection, OVA_{488}-derived signals were mainly scattered in the $Ly51^+$ cortical area but not in the I-$A^{d\ high}$ medullary area (Fig. 5*E*). Because OVA_{488}-derived signals were constantly detected in Sirpα^+ DCs at every time point (data not shown), these observations suggest that Sirpα^+ DCs initially capture bloodstream OVA protein inside PVRs or in nearby small vessels and then migrate into the cortical parenchyma. To examine the process of migration more in detail, OVA_{647} (blue) and OVA_{488} (green) were i.v. injected sequentially with an interval of either 6 or 18 h as shown in Fig. 5*F*. When OVA_{488} was injected 6 h after OVA_{647}, double-positive $CD11c^{high}$ DCs were evidently detected (8.1%), while single-positive cells were sparse (Fig. 5*F*, *left upper panel*). Even at 18 h after the injection, double-positive $CD11c^{high}$ DCs were still

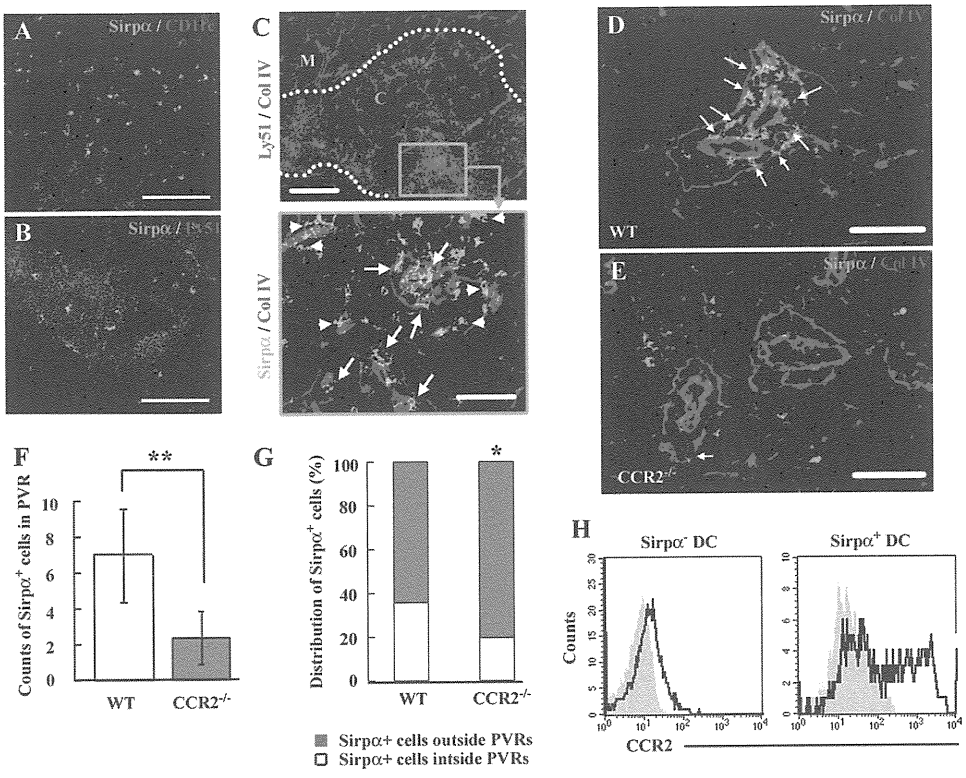

FIGURE 3. Localization of thymic Sirpα^+ DCs. Double-color fluorescence immunostaining for Sirpα (green) and CD11c (red; *A*), Ly51 (red; *B*), or Col IV (red; *D* and *E*). *C*, Triple-color fluorescent immunostaining for Sirpα (green), Ly51 (red), and Col IV (blue). Low magnification image for Ly51 and Col IV is shown in the *upper panel*. A green square in the *upper panel* is observed at a higher magnification for Col IV and Sirpα expression and is shown in the *lower panel*. Dashed lines indicate the boundary between cortex (C) and medulla (M). Arrowheads in *C* and arrows in *C–E* indicate Sirpα^+ cells interacting with small vessels and inside the PVRs, respectively. *A–D*, WT thymus. *E*, CCR2$^{-/-}$ thymus. Representative results from at least two independent experiments are shown here. Scale bars: *A* and *B*, 100 μm; *upper panel* of *C*, 200 μm; *lower panel* of *C–E*, 50 μm. *F* and *G*, At least five photographs in the central regions of the PVRs were taken at $\times$200 magnification in each tissue sample. The numbers of Sirpα^+ cells inside the PVRs were determined and data represent mean $\pm$ SD of three independent experiments. **, $p < 0.01$. *F*, The proportion of Sirpα^+ cells inside the PVRs to outside was calculated and data represent the mean of three independent experiments. *, $p < 0.05$ (*G*). *H*, CCR2 expression on CD11c^{high}Sirpα^- or Sirpα^+ cDCs. Gray-filled and black-open histograms indicate the results from isotype control and specific mAb for CCR2, respectively. Representative results from three independent experiments are shown here.

present (3.2%) with substantial numbers of OVA_{488}-derived signal single-positive (3.9%) or OVA_{647}-derived signal single-positive cells (2.3%; Fig. 5*F*, *left lower panel*). Thus, CD11c^{high} DCs with Sirpα expression can persistently be in close interaction with the bloodstream while they are migrating into cortical parenchyma (Fig. 5*G*).

Depressed migration of Sirpα^+ DCs and their aberrant intrathymic localization in CCR2$^{-/-}$ mice

It is possible that a decreased intrathymic Sirpα^+ DC number may account for the defect in their migration in CCR2$^{-/-}$ mice, because the thymic Sirpα^+ cDC subset is presumed to migrate from the bloodstream (14). Most CD11c$^+$B220$^-$ DCs in peripheral blood and bone marrow expressed abundantly Sirpα (supplemental Fig. S4), similarly as observed on thymic Sirpα^+ DCs, and this population expressed CCR2 (supplemental Fig. S5). CCR2$^{-/-}$ mice exhibited a moderate reduction in CD11c$^+$B220$^-$ DCs in peripheral blood, but not bone marrow (Fig. 6, *A* and *B*). This suggests a possible defect in the migration of CD11c$^+$B220$^-$ DCs from bone marrow in CCR2$^{-/-}$ mice. To test this possibility, bone marrow cells were induced to differentiate to DCs with in vitro GM-CSF stimulation, labeled with CMFDA, and injected into bone marrow of WT mice (Fig. 6*C*, *upper illustration*). Under these conditions, >80% of injected cells expressed CD11c, Sirpα, and CCR2, but not B220 (supplemental Figs. S4 and S5). WT-derived DCs appeared in peripheral blood rapidly within 2 h after the intra-bone marrow injection, whereas CCR2$^{-/-}$ mouse-derived DCs migrated into peripheral blood less efficiently (Fig. 6, *C* and *D*). Interestingly, CD11c$^+$B220$^-$Sirpα^+ DCs appeared in thymus by 6 h after intra-bone marrow injection (Fig. 6*E*). These observations suggest that CCR2-mediated signals were critical of the migration of Sirpα^+ DCs from bone marrow into the thymus. Moreover, Sirpα^+ DCs were markedly decreased in PVRs of CCR2$^{-/-}$ thymus compared with those of WT thymus (WT mice, 7.0 $\pm$ 2.6/site; CCR2$^{-/-}$ mice, 2.3 $\pm$ 1.5/site; Fig. 3, *D–F*). Furthermore, the decrease was more evident in the region inside the PVRs compared with that outside the PVRs (Fig. 3*G*). CCR2 was expressed also by a portion of intrathymic Sirpα^+ DCs, but not Sirpα^- DCs (Fig. 3*H*). Three mouse chemokines, MCP-1, MCP-2, and MCP-3, can bind to CCR2 (30). Among these chemokines, only MCP-2 mRNA was constitutively expressed in thymus, particularly keratin 8-positive thymic stroma, but not CD45-positive thymocytes (Fig. 7, *A* and *B*). Moreover, MCP-2 immunoreactivities were consistently detected inside the PVRs (Fig. 7*C*, *upper panels*) and on Sirpα^+ cells in the PVRs (Fig. 7*C*, *lower panels*). Thus, it is probable that the CCR2-MCP-2 interaction can contribute to intrathymic localization of Sirpα^+ DCs, particularly in the PVRs.

Defective Ag uptake by Sirpα^+ DCs in CCR2$^{-/-}$ mice

Because the PVR was proved to be a main location of the uptake of circulating Ags, we further examined the effects of CCR2

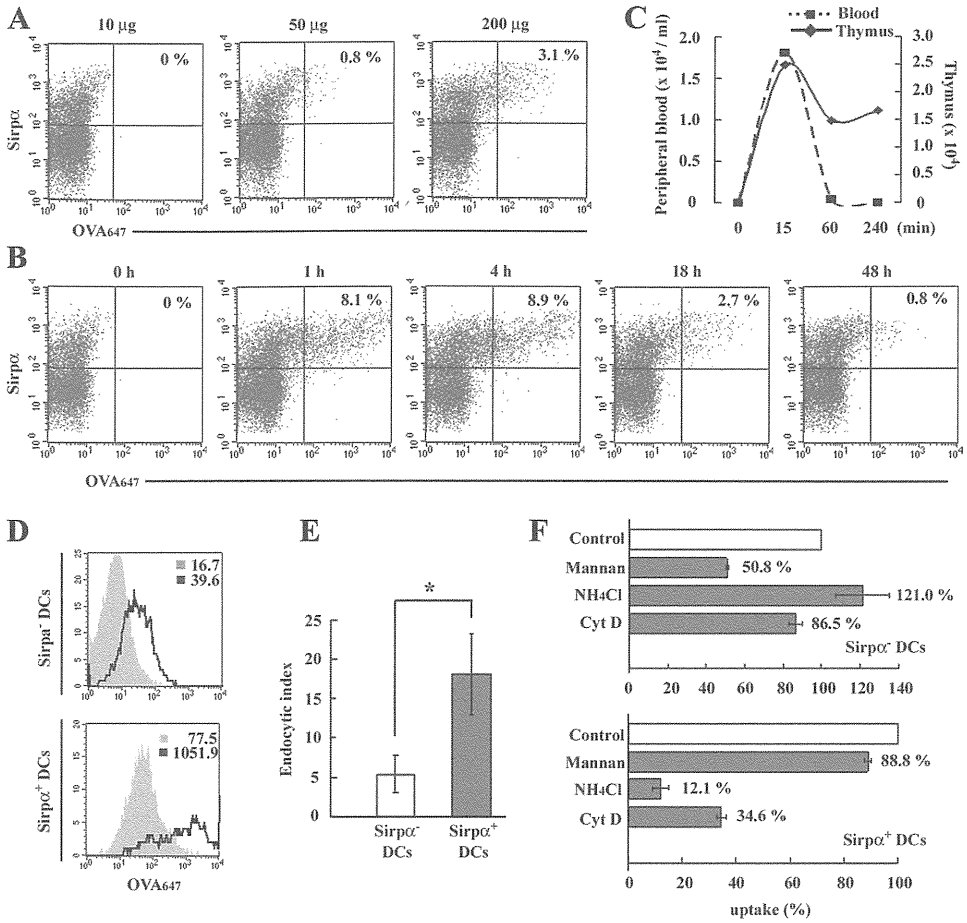

FIGURE 4. Uptake of bloodstream Ag by thymic Sirpα+ DCs. *A*, At 18 h after injection with OVA_{647} at the indicated doses, low-density cells were isolated from WT thymus and were stained with anti-CD11c and anti-Sirpα mAbs. Then the uptake of OVA_{647} in the $CD11c^{high}$ DC population was analyzed. *B*, Uptake of OVA_{647} at the indicated time points. OVA_{647} (200 μg) was injected into the tail vein. Percentage of $Sirp\alpha^+OVA_{647}^+$ region is shown in each panel of *A* and *B*. Representative results from three independent experiments are shown. *C*, Time kinetics of the numbers of DCs capturing OVA protein in the peripheral blood (broken line) and thymus (solid line). *D*, In vitro endocytosis of OVA_{647} by $CD11c^{high}Sirp\alpha^-$ and $CD11c^{high}Sirp\alpha^+$ cDCs are shown in the *upper* and *lower panels*, respectively. Gray-filled and black-open histograms indicate the results obtained when the cells were incubated at 0 and 37°C, respectively. Numbers in each panel indicates mean fluorescence intensity for OVA_{647} captured. Representative results from three independent experiments are shown here. *E*, Endocytic index in $Sirp\alpha^-$ and $Sirp\alpha^+$ cDCs. Endocytic index was calculated as mean fluorescence intensity at 37°C/mean fluorescence intensity at 0°C. Mean ± SD were calculated from three independent experiments and are shown here. *, $p < 0.01$. *F*, The effects of various agents on endocytosis. Uptake in the presence of each inhibitor is shown as the percentage of total uptake in the absence of any inhibitors. Means were calculated from three independent experiments and are shown here.

deficiency on the capability of $Sirp\alpha^+$ DCs to uptake Ags from the bloodstream. Indeed, when OVA_{647} was injected i.v., $CCR2^{-/-}$ mice exhibited a reduced proportion of intrathymic DCs capturing OVA protein compared with WT mice (Fig. 8, *A* and *B*). Moreover, after the OVA_{647} injection, $Sirp\alpha^+$ DCs of WT mice contained a substantial proportion of OVA^{high} cells, which represent the cells with a higher uptake of OVA protein, and this population was markedly reduced in $CCR2^{-/-}$ mice (Fig. 8, *C* and *D*). Moreover, among $Sirp\alpha^+$ DCs, the CCR2-expressing population was a main cell type which captured OVA protein (Fig. 8*E*). CMFDA-labeled WT mouse-derived bone marrow cells appeared in thymus 2 days after the adoptive transfer to CCR2-deficient mice and a substantial proportion of these stained cells expressed CD11c and Sirpα simultaneously (Fig. 8*F*). $Sirp\alpha^+CD11c^+$ DCs appeared in thymus similarly when CMFDA-labeled CCR2-deficient mouse-derived bone marrow cells were adoptively transferred (data not shown). When OVA_{647} was injected i.v. 2 days after the adoptive transfer, WT donor-derived $Sirp\alpha^+CD11c^+$ DCs captured OVA protein more efficiently than CCR2-deficient DCs in the CCR2-deficient thymus (Fig. 8*G*). Thus, CCR2-mediated signals may at least partially regulate the function of $Sirp\alpha^+$ DCs to uptake Ag from the bloodstream (supplemental Fig. S6).

Accumulation of autoreactive T cells against serum Ags in the periphery of $CCR2^{-/-}$ mice

We observed that $CCR2^{-/-}$ mice did not exhibit any signs suggestive of autoimmune disorders until 1 year after the birth (our unpublished data). Hence, we examined whether autoreactive T cells against certain self-Ags in the bloodstream accumulated in the periphery of $CCR2^{-/-}$ mice. We examined the accumulation of autoreactive T cells in the draining lymph nodes in WT mice that received CFSE-labeled WT or $CCR2^{-/-}$ mouse-derived splenocytes and were subsequently immunized with mouse serum emulsified in CFA. Immunization with total serum protein increased the cell division of $CCR2^{-/-}$ mouse-derived $CD4^+$ T cells inside draining lymph nodes (10.6%) to a greater extent than immunization with PBS (4.3%; Fig. 9*A*). Moreover, $CD4^+$ T cell division was significantly increased in the recipients of $CCR2^{-/-}$ mouse-derived splenocytes compared with the recipients of WT mouse-derived splenocytes (Fig. 9*B*). Thus, the lack of CCR2 can

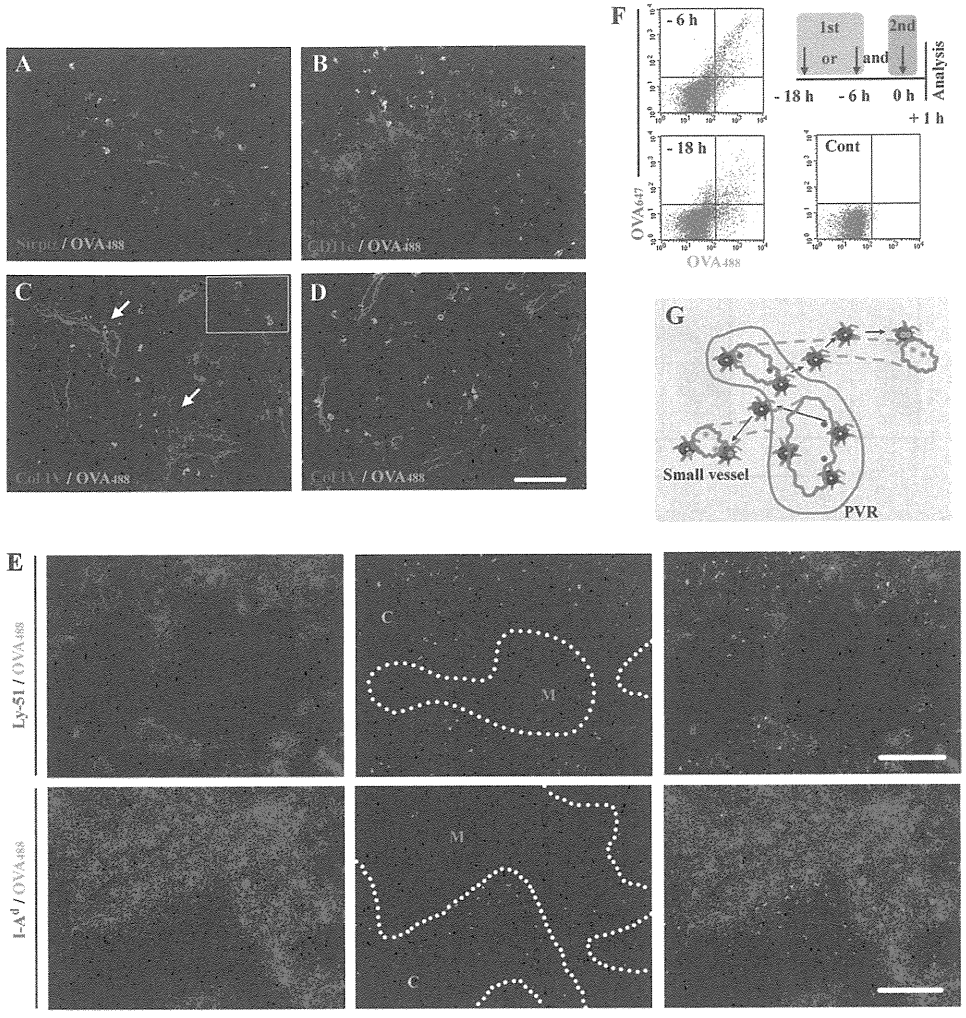

FIGURE 5. Localization of i.v. injected Ag in thymus. *A–C*, Thymic tissues were obtained 0.5 h after injection of OVA_{488} and were stained to obtain a double-color fluorescent image with the combination of OVA_{488} (green) and (*A*) Sirpα (red), (*B*) CD11c (red), or (*C*) Col IV (red). Arrows in *C* indicate the cells with captured OVA_{488} inside the PVRs. The image showing the cells capturing OVA_{488} in close proximity to small vessels is an *inset* in *C*. *D*, A double-color fluorescent image for OVA_{488} (green) and Col IV (red) at 6 h after OVA injection. Scale bars, 100 μm. *E*, A double-color fluorescent image with the combination of OVA_{488} (green) and Ly51 (red) or I-A^d (red) at 18 h after injection is shown in the *upper* and *lower panels*, respectively. The merged images are shown in the *right panels*. Dashed lines indicate the boundary between cortex (C) and medulla (M). Scale bars, 200 μm. *F*, OVA_{647} and OVA_{488} were i.v. injected consequently with an interval of either 6 or 18 h, illustrated in *upper right panel* in *F*. Uptake of OVA protein by $CD11c^{high}$ DC population isolated after double injection with an interval of either 6 or 18 h is shown in the *left upper* and *lower panels*, respectively. Autofluorescence for each parameter in the $CD11c^{high}$ DC population without injection is shown as a control. Representative results from three independent experiments are shown here. *G*, Presumed intrathymic trafficking modes of Sirpα^+ DCs, combined with the Ag uptake. Blue and green particles indicate OVA_{647} and OVA_{488}, respectively.

result in enhanced accumulation of autoreactive T cells against serum self-Ags.

Discussion

Mouse thymus $CD11c^+$ cDCs can be classified into two populations, a major $CD8\alpha^+$ and a minor $CD8\alpha^-$ one (31). $CD8\alpha^-$ cDCs can pick up $CD8\alpha\beta$ heterodimer from thymocytes and retain them on the cell surface, thus precluding the use of $CD8\alpha$ as a reliable marker to distinguish these two populations. Wu and Shortman (8) observed that $CD8\alpha^-$ but not $CD8\alpha^+$ cDCs simultaneously express the Sirpα molecule and proposed the use of Sirpα as a marker of this minor cDC population. Concomitantly, it was proposed that the interaction between thymocytes and DCs in thymic cortex can also have profound effects on positive selection (32). Likewise, McCaughtry et al. (33) observed that clonal deletion of autoreactive thymocytes requires the stimuli from rare $CD11c^+$ cortical DCs. Given the unique localization of Sirpα^+ DCs confined to the cortex, these observations suggest the potential involvement of Sirpα^+ DCs in central tolerance, but their small number hinders the isolation for a detailed analysis of Sirpα^+ DC function.

A partial but selective reduction in intrathymic Sirpα^+ cDCs in $CCR2^{-/-}$ mice prompted us to investigate the thymic selection process in WT and $CCR2^{-/-}$ mice to elucidate the role of intrathymic Sirpα^+ cDCs in the process. When DO11.10 TCR-transgenic mice were administered immunogenic $OVA_{323-339}$ peptide i.v., *CCR2* gene ablation partially attenuated the clonal negative deletion by apoptosis of the $DO11.10^+$ DP thymocyte population. Intraperitoneal injection of anti-CD3 Ab deleted thymocytes to similar extents in WT and $CCR2^{-/-}$ mice, excluding the possibility that CCR2 deficiency impaired the apoptotic response of thymocytes. Negative selection can be exerted by various types of APCs including Sirpα^- cDCs, B cells, macrophages, cortical thymic epithelial cells, and mTEC in addition to Sirpα^+ cDCs. We

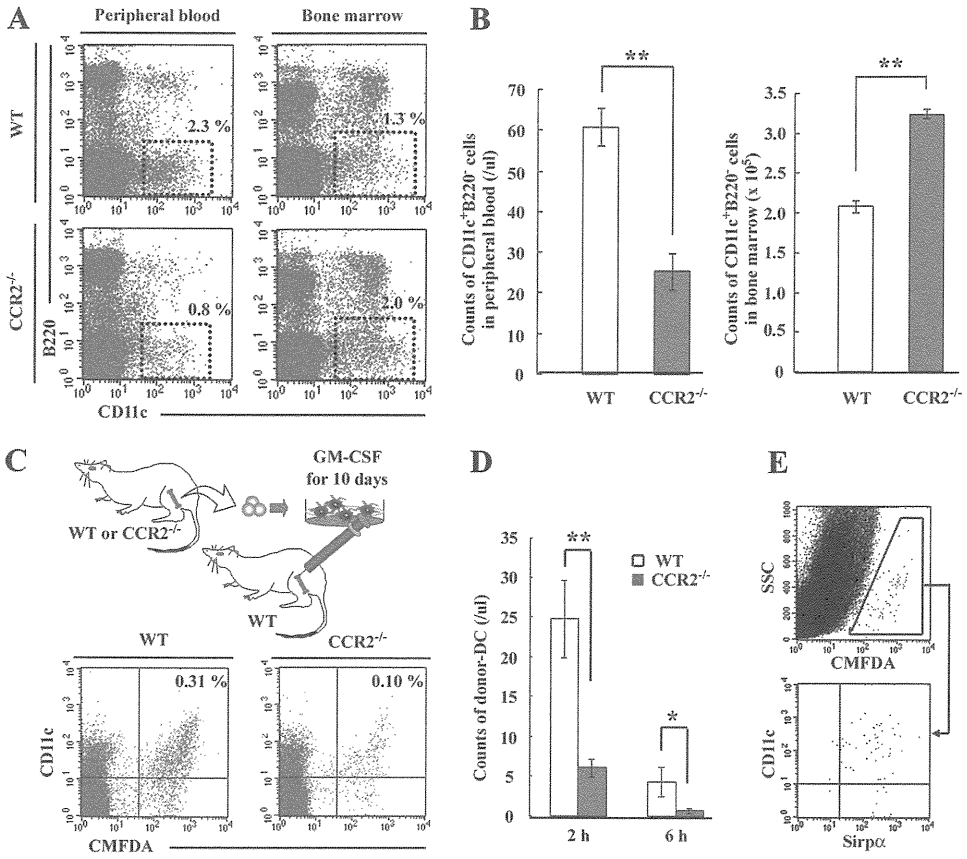

FIGURE 6. Mobilization of Sirpα$^+$ DCs from bone marrow. *A* and *B*, PBMCs and bone marrow cells isolated from femur bone marrow were stained with anti-CD11c and anti-B220 mAbs. Proportion (*A*) and the numbers (*B*) of CD11c$^+$B220$^-$ cells gated with the dot squares were determined on peripheral blood and bone marrow in CCR2$^{-/-}$ and WT mice. Percentage of gated cells is shown in each panel of *A*. Mean ± SD were calculated from three independent experiments and are shown here. *C*, The image of experimental procedure of "trafficking of bone marrow-derived DCs" was illustrated and is shown in the *upper panel*. PBMCs were isolated from the recipients 2 h after injection and stained with anti-CD11c mAb. Egress of CCR2$^{-/-}$ bone marrow-derived DCs into peripheral blood was compared with WT DCs. Percentage of donor DCs in CMFDA$^+$CD11c$^+$ region is shown in each panel. *D*, The numbers of donor-derived DCs in peripheral blood were determined 2 and 6 h after injection. Mean ± SD calculated from five independent experiments are shown here. *, $p < 0.05$ and **, $p < 0.01$. *E*, One × 10^7 WT bone marrow cell-derived DCs were injected into both the right and left tibial cavity. Six hours after injection, expression of Sirpα and CD11c on intrathymic migrated CMFDA$^+$ donor cells was analyzed by FCM. Representative results from four independent experiments are shown here.

failed to detect any apparent differences in other APC populations than Sirpα$^+$ cDCs between WT and CCR2$^{-/-}$ mice. Thus, it is unlikely that reduced negative selection in CCR2$^{-/-}$ mice can be ascribed to the changes in these cell populations. Furthermore, accumulating evidence implicates intrathymic CD4$^+$CD25$^+$ regulatory T cells as an essential cell component in central tolerance.

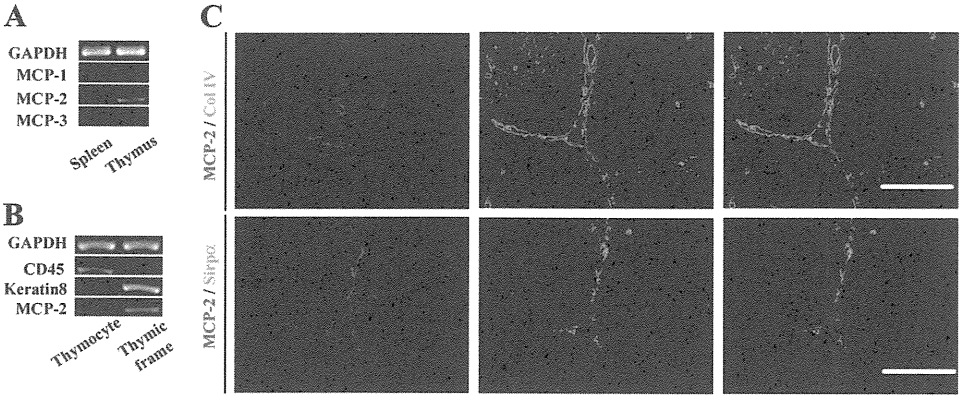

FIGURE 7. Expression of CCR2 ligands in thymus under physiological condition. *A*, Total RNAs were extracted from thymus and spleen of WT mice. Expression of CCR2 ligands, MCP-1, MCP-2, and MCP-3, was determined by RT-PCR. GAPDH served as an internal positive control. *B*, Thymic tissues were mechanically disrupted and fractionated into thymocyte and thymic stromal components. MCP-2 transcripts were determined on these two fractions by RT-PCR. CD45 and keratin 8 served as positive control for the thymocyte and thymic stromal fraction, respectively. *C*, Double-color fluorescent immunostaining for MCP-2 (red) and Col IV (green) or MCP-2 (red) and Sirpα (green) in the thymic tissue sections are shown in the *upper* and *lower panels*, respectively. The merged images are shown in the *right panels*. Representative results from three independent animals are shown here. Scale bars, 100 μm.

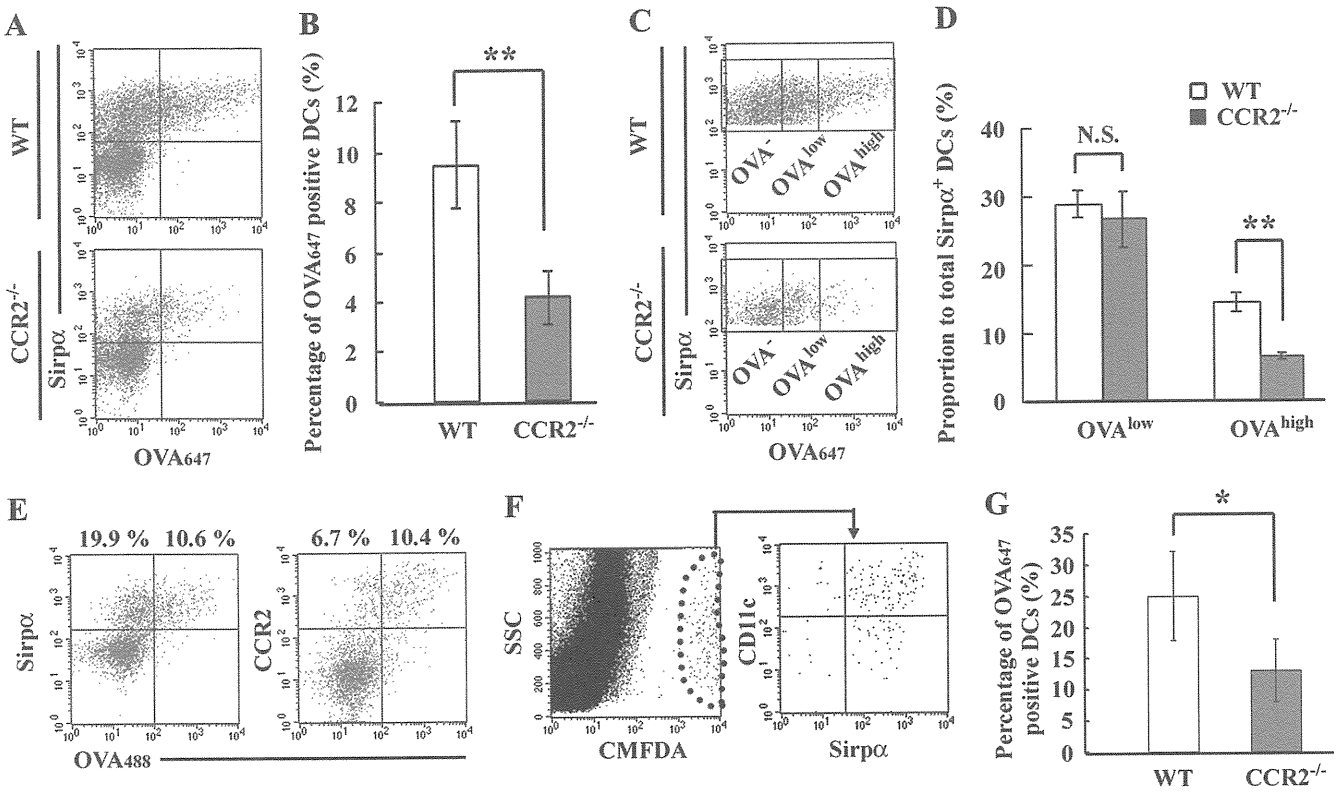

FIGURE 8. Effects of CCR2 deficiency on Ag uptake by thymic Sirpα^+ DCs. *A*, The uptake of OVA_{647} in the CCR2$^{-/-}$ CD11c^{high} DC population at 4 h after i.v. injection was compared with WT-derived cells. *B*, Percentage of DCs capturing OVA_{647} in the CD11c^{high} DC population. Mean ± SD were calculated from five independent experiments and are shown here. **, $p < 0.01$ *C*, Sirpα^+ DCs derived from WT and CCR2$^{-/-}$ thymus were separated into three groups according to the efficiency of OVA_{647} uptake, OVA$^-$; DCs without capturing OVA_{647}, OVA^{low}; DCs capturing OVA_{647} with a low efficiency, and OVA^{high}; and DCs capturing OVA_{647} with a high efficiency. *D*, Percentage of OVA^{low} and OVA^{high} in WT and the CCR2$^{-/-}$ Sirpα^+ DC population. Mean ± SD were calculated from five independent experiments and are shown here. **, $p < 0.01$; N.S., no significant difference. *E*, OVA_{488} was i.v. injected into WT mice. One hour after injection, low-density cells were stained with anti-CD11c and anti-Sirpα or anti-CCR2 mAbs. The uptake of OVA_{488} and expression of Sirpα or CCR2 in the CD11c^{high} DC population are shown. Percentage of Sirpα^+OVA$_{488}^+$ and OVA$_{488}^-$, or CCR2$^+$OVA$_{488}^+$ and OVA$_{488}^-$ regions are shown in the *left* or *right panel*. Representative results from three independent experiments are shown here. *F*, Migration of Sirpα^+ DCs into the thymus at 2 days after i.v. injection of CMFDA-labeled WT bone marrow cells into CCR2$^{-/-}$ mice. Expression of CD11c and Sirpα on CMFDA$^+$ donor-derived cells is shown in the *right panel*. Representative results from three independent experiments are shown here. *G*, OVA_{647} was i.v. injected into CCR2$^{-/-}$ mice at 2 days after injection of bone marrow cells. Percentage of WT and CCR2$^{-/-}$ donor-derived DCs capturing OVA_{647} in the CMFDA$^+$CD11c^{high} region are shown. Mean ± SD were calculated from four independent experiments and are shown here. *, $p < 0.05$.

Indeed, Proietto et al. (14) recently reported the capability of Sirpα^+ cDCs to induce the differentiation of regulatory T cells in vitro. However, OVA peptide injection induced the differentiation of regulatory T cells to similar extents in both DO11.10 and DO11.10/CCR2$^{-/-}$ thymus. Thus, it is probable that CCR2 deficiency reduced modestly intrathymic Sirpα^+ DCs without affecting regulatory cell induction and partially attenuated negative selection in vivo.

It remains elusive on the trafficking modes of Sirpα^+ DCs. In CCR2$^{-/-}$ mice, Sirpα^+ DCs were decreased moderately in peripheral blood and thymus, but were increased in bone marrow. Considering that CCR2 signaling can regulate the mobilization of monocytes from bone marrow to peripheral blood (34, 35), these observations raised the possibility of a defect in the trafficking of Sirpα^+ DCs from bone marrow in CCR2$^{-/-}$ mice. Indeed, WT mouse-derived Sirpα^+ DCs, injected into bone marrow, appeared first in peripheral blood and then the thymus. On the contrary, CCR2$^{-/-}$ mouse-derived Sirpα^+ DCs exhibited impairment in the egress from bone marrow to peripheral blood. These observations suggest that bone marrow-derived Sirpα^+ DCs migrated to peripheral blood in response to CCR2-mediated signals and subsequently traffic to the thymus.

In the thymus, Sirpα^+ DCs were characteristically localized in close proximity to small blood vessels and inside the PVRs, sites which are compartmentalized by a vascular basement membrane and a border membrane separating them from the thymic parenchyma (36). It is of note that Sirpα^+ cells in the PVRs were markedly decreased in CCR2$^{-/-}$ mice to a greater extent than the decrease in total Sirpα^+ cell number. Thus, intrathymic CCR2 signaling can regulate their unique localization. This notion was supported by the observation that MCP-2, a potential ligand for CCR2, was constitutively detected in the PVRs, where Sirpα^+ DCs were present.

PVRs can provide a pathway for hematopoietic progenitor cells and mature T cells to traverse from the bloodstream to the thymic parenchyma (36) and are presumed to constitute the blood-thymus barrier, which can protect the thymic parenchyma from bloodstream-derived macromolecules (28). Thus, the unique localization of Sirpα^+ cDCs in the thymus suggested their potential interactions with bloodstream-derived Ag. This assumption was strengthened by our present observation that intrathymic Sirpα^+ cDCs rapidly and specifically captured OVA protein and serum IgG following i.v. injection. Moreover, injected Ags were initially detected inside PVRs or in nearby small vessels and were subsequently in the cortical parenchyme, and the injected Ag-derived

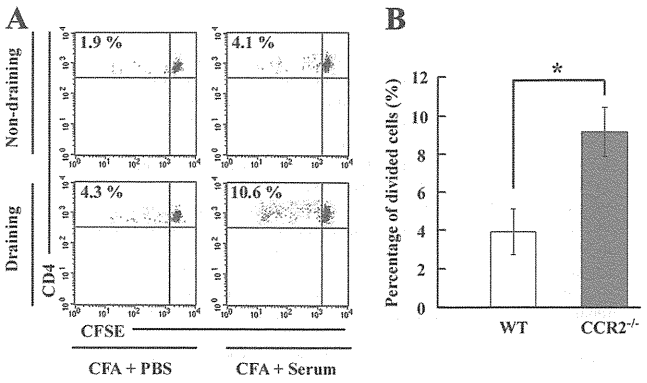

FIGURE 9. Accumulation of autoreactive T cells against serum Ags in the spleen. Spleen mononuclear cells were isolated from WT or CCR2$^{-/-}$ mice and i.v. injected into WT mice after labeling with CFSE. *A*, Recipients of CCR2$^{-/-}$ mouse-derived splenocytes were immunized with total mouse serum or PBS emulsified in CFA at 1 day after injection. Four days after, draining and nondraining lymph nodes were harvested and division of CFSE$^+$ donor-derived CD4$^+$ T cells was analyzed by FCM. Representative results from three independent experiments are shown here. *B*, Percentage of divided CD4$^+$ T cells was determined in the draining lymph nodes of the recipients of either WT-derived or CCR2$^{-/-}$ donor-derived splenocytes when the recipients were immunized with mouse serum emulsified in CFA. Mean ± SD were calculated from three independent experiments and are shown here. *, $p < 0.01$.

signals were consistently colocalized with CD11c and Sirpα. Thus, after CD11c$^+$Sirpα$^+$ cDCs, located around the PVRs, capture the Ags, they presumably move to cortical parenchyme to educate T cells. Indeed, CCR2$^{-/-}$ thymus-derived Sirpα$^+$ DCs exhibited a reduced capacity to uptake OVA. The lack of CCR2 can hinder the proper intrathymic localization of Sirpα$^+$ DCs and their distinctive function, Ag uptake from bloodstream, thereby reducing Ag presentation in the cortical parenchyma and subsequent negative selection against a blood-borne Ag. This hypothesis is supported by our observation in that CD4$^+$ T cells reactive to certain serum self-Ags accumulated in the periphery of the recipients of CCR2$^{-/-}$ mouse-derived splenocytes to a greater extent than the recipients of WT mouse-derived splenocytes.

DCs can uptake free soluble Ags, in three distinct manners, by clathrin-mediated endocytosis, nonclathrin/caveolae endocytosis, and macropinocytosis (25). Thymic Sirpα$^+$ cDCs could endocytose OVA Ags more efficiently than thymic Sirpα$^-$ cDCs when they were cultured in vitro with OVA Ags. Furthermore, NH_4Cl, an inhibitor of clathrin-mediated endocytosis (26), markedly inhibited OVA endocytosis by Sirpα$^+$ cDCs, but not by Sirpα$^-$ cDCs. On the contrary, OVA protein endocytosis by Sirpα$^-$ DCs was partially inhibited by mannan, whereas mannan had few effects on OVA protein endocytosis by Sirpα$^+$ DCs. These observations suggest that thymic Sirpα$^+$ cDCs characteristically can efficiently endocytose Ags in a manner distinct from thymic Sirpα$^-$ cDCs.

Balazs et al. (29) reported that bloodstream DCs could efficiently capture and transport particulate bacteria into the spleen when particulate bacteria were i.v. injected. We also observed that CD11c$^+$ DCs rapidly disappeared from peripheral blood after uptake of i.v. injected OVA protein. Given the capacity of CD11c$^+$ DCs to move rapidly from blood to thymus, blood CD11c$^+$ DCs may migrate into thymus after capturing the i.v. injected Ag. However, Ag-capturing DCs appeared very rapidly in the thymus, reaching maximal levels before disappearance of Ag-capturing circulating DCs from the peripheral blood. Furthermore, when OVA protein was injected i.v. into mice that contained bloodstream DCs labeled with fluorescent-conjugated latex beads, latex-labeled DCs did not appear in the thymus (our unpublished data). Thus, it is remotely possible that bloodstream DCs captured OVA protein and subsequently migrated into thymus.

In this study, we identified the unique intrathymic localization and functions of thymic Sirpα$^+$ DCs that are involved in negative selection, particularly against blood-borne Ags. Serum protein can also induce negative selection in thymus (27, 37) but the molecular and cellular mechanisms remain to be elucidated. Because Sirpα$^+$ cDCs can uptake serum protein such as IgG, these cells may induce central tolerance to blood-borne-derived Ags, in addition to Ags presented by the well-characterized intrathymic AIRE-mediated pathway.

We have shown that CCR2-mediated signals can regulate various biological aspects of Sirpα$^+$ DCs such as their appropriate intrathymic localization and Ag uptake capacity. It is widely held that CCR2 might be a potential therapeutic target for several autoimmune disorders. However, because CCR2-mediated signals may contribute to thymic negative selection against blood-borne Ags, CCR2 blockade may aggravate autoimmune disorders similar to the observation on the murine collagen-induced arthritis model (38). Moreover, Lauritzsen et al (39) reported that proteins secreted from tumor cells into peripheral blood were transported into the thymus to eventually cause clonal deletion of tumor Ag-specific T cell repertoires. Given the potential capacity of intrathymic Sirpα$^+$ DCs to capture blood-borne Ags, they may have a role in the development of tumor tolerance. Because human thymus contains DCs with similar phenotypes and intrathymic localization as Sirpα$^+$ cDCs (40), a more detailed elucidation of the functions of Sirpα$^+$ cDCs may provide us with useful insights to develop a better therapeutic strategy for cancer and stem cell transplantation as well as autoimmune disorders.

Acknowledgments

We express our gratitude to Drs. Joost J. Oppenheim (National Cancer Institute-Frederick, Frederick, MD) and Nobuyuki Onai (Akita University, Akita, Japan), and Yi Zhang (University of Michigan, Ann Arbor, MI) for critical review of this manuscript. We thank Drs. William Kuziel, Kouji Matsushima, and Philip Murphy for providing us with CCR2-, CCR5-, and CCR1- and CX3CR1-deficient mice, respectively.

Disclosures

The authors have no financial conflict of interest.

References

1. von Boehmer, H., I. Aifantis, F. Gounari, O. Azogui, L. Haughn, I. Apostolou, E. Jaeckel, F. Grassi, and L. Klein. 2003. Thymic selection revisited: how essential is it? *Immunol. Rev.* 191: 62–78.
2. Anderson, M. S., E. S. Venanzi, Z. Chen, S. P. Berzins, C. Benoist, and D. Mathis. 2005. The cellular mechanism of Aire control of T cell tolerance. *Immunity* 23: 227–239.
3. Anderson, M. S., E. S. Venanzi, L. Klein, Z. Chen, S. P. Berzins, S. J. Turley, H. von Boehmer, R. Bronson, A. Dierich, C. Benoist, and D. Mathis. 2002. Projection of an immunological self shadow within the thymus by the aire protein. *Science* 298: 1395–1401.
4. Liston, A., S. Lesage, J. Wilson, L. Peltonen, and C. C. Goodnow. 2003. Aire regulates negative selection of organ-specific T cells. *Nat. Immunol.* 4: 350–354.
5. Anderson, G., K. M. Partington, and E. J. Jenkinson. 1998. Differential effects of peptide diversity and stromal cell type in positive and negative selection in the thymus. *J. Immunol.* 161: 6599–6603.
6. Marrack, P., D. Lo, R. Brinster, R. Palmiter, L. Burkly, R. H. Flavell, and J. Kappler. 1988. The effect of thymus environment on T cell development and tolerance. *Cell* 53: 627–634.
7. Matzinger, P., and S. Guerder. 1989. Does T-cell tolerance require a dedicated antigen-presenting cell? *Nature* 338: 74–76.
8. Wu, L., and K. Shortman. 2005. Heterogeneity of thymic dendritic cells. *Semin. Immunol.* 17: 304–312.
9. Liu, Y. J. 2006. A unified theory of central tolerance in the thymus. *Trends Immunol.* 27: 215–221.
10. Bendriss-Vermare, N., C. Barthelemy, I. Durand, C. Bruand, C. Dezutter-Dambuyant, N. Moulian, S. Berrih-Aknin, C. Caux, G. Trinchieri, and F. Briere. 2001. Human

thymus contains IFN-α-producing CD11c$^-$, myeloid CD11c$^+$, and mature interdigitating dendritic cells. *J. Clin. Invest.* 107: 835–844.
11. Sprent, J., and S. R. Webb. 1995. Intrathymic and extrathymic clonal deletion of T cells. *Curr. Opin. Immunol.* 7: 196–205.
12. Heino, M., P. Peterson, N. Sillanpaa, S. Guerin, L. Wu, G. Anderson, H. S. Scott, S. E. Antonarakis, J. Kudoh, N. Shimizu, et al. 2000. RNA and protein expression of the murine *autoimmune regulator gene (Aire)* in normal, RelB-deficient and in NOD mouse. *Eur. J. Immunol.* 30: 1884–1893.
13. Kyewski, B., and J. Derbinski. 2004. Self-representation in the thymus: an extended view. *Nat. Rev. Immunol.* 4: 688–698.
14. Proietto, A. I., S. van Dommelen, P. Zhou, A. Rizzitelli, A. D'Amico, R. J. Steptoe, S. H. Naik, M. H. Lahoud, Y. Liu, P. Zheng, et al. 2008. Dendritic cells in the thymus contribute to T-regulatory cell induction. *Proc. Natl. Acad. Sci. USA* 105: 19869–19874.
15. Heinzel, K., C. Benz, and C. C. Bleul. 2007. A silent chemokine receptor regulates steady-state leukocyte homing in vivo. *Proc. Natl. Acad. Sci. USA* 104: 8421–8426.
16. Kim, C. H. 2005. The greater chemotactic network for lymphocyte trafficking: chemokines and beyond. *Curr. Opin. Hematol.* 12: 298–304.
17. Schutyser, E., A. Richmond, and J. Van Damme. 2005. Involvement of CC chemokine ligand 18 (CCL18) in normal and pathological processes. *J. Leukocyte Biol.* 78: 14–26.
18. Vecchi, A., L. Massimiliano, S. Ramponi, W. Luini, S. Bernasconi, R. Bonecchi, P. Allavena, M. Parmentier, A. Mantovani, and S. Sozzani. 1999. Differential responsiveness to constitutive vs. inducible chemokines of immature and mature mouse dendritic cells. *J. Leukocyte Biol.* 66: 489–494.
19. Niess, J. H., S. Brand, X. Gu, L. Landsman, S. Jung, B. A. McCormick, J. M. Vyas, M. Boes, H. L. Ploegh, J. G. Fox, et al. 2005. CX3CR1-mediated dendritic cell access to the intestinal lumen and bacterial clearance. *Science* 307: 254–258.
20. Gao, J. L., T. A. Wynn, Y. Chang, E. J. Lee, H. E. Broxmeyer, S. Cooper, H. L. Tiffany, H. Westphal, J. Kwon-Chung, and P. M. Murphy. 1997. Impaired host defense, hematopoiesis, granulomatous inflammation and type 1-type 2 cytokine balance in mice lacking CC chemokine receptor 1. *J. Exp. Med.* 185: 1959–1968.
21. Combadiere, C., S. Potteaux, J. L. Gao, B. Esposito, S. Casanova, E. J. Lee, P. Debre, A. Tedgui, P. M. Murphy, and Z. Mallat. 2003. Decreased atherosclerotic lesion formation in CX3CR1/apolipoprotein E double knockout mice. *Circulation* 107: 1009–1016.
22. Murai, M., H. Yoneyama, T. Ezaki, M. Suematsu, Y. Terashima, A. Harada, H. Hamada, H. Asakura, H. Ishikawa, and K. Matsushima. 2003. Peyer's patch is the essential site in initiating murine acute and lethal graft-versus-host reaction. *Nat. Immunol.* 4: 154–160.
23. Kuziel, W. A., S. J. Morgan, T. C. Dawson, S. Griffin, O. Smithies, K. Ley, and N. Maeda. 1997. Severe reduction in leukocyte adhesion and monocyte extravasation in mice deficient in CC chemokine receptor 2. *Proc. Natl. Acad. Sci. USA* 94: 12053–12058.
24. Brewer, J. A., O. Kanagawa, B. P. Sleckman, and L. J. Muglia. 2002. Thymocyte apoptosis induced by T cell activation is mediated by glucocorticoids in vivo. *J. Immunol.* 169: 1837–1843.
25. Mayor, S., and R. E. Pagano. 2007. Pathways of clathrin-independent endocytosis. *Nat. Rev. Mol. Cell Biol.* 8: 603–612.
26. Sandvig, K., S. Olsnes, O. W. Petersen, and B. van Deurs. 1987. Acidification of the cytosol inhibits endocytosis from coated pits. *J. Cell Biol.* 105: 679–689.
27. Zal, T., A. Volkmann, and B. Stockinger. 1994. Mechanisms of tolerance induction in major histocompatibility complex class II-restricted T cells specific for a blood-borne self-antigen. *J. Exp. Med.* 180: 2089–2099.
28. Bubanovic, I. V. 2003. Failure of blood-thymus barrier as a mechanism of tumor and trophoblast escape. *Med. Hypotheses* 60: 315–320.
29. Balazs, M., F. Martin, T. Zhou, and J. Kearney. 2002. Blood dendritic cells interact with splenic marginal zone B cells to initiate T-independent immune responses. *Immunity* 17: 341–352.
30. Murphy, P. M., M. Baggiolini, I. F. Charo, C. A. Hebert, R. Horuk, K. Matsushima, L. H. Miller, J. J. Oppenheim, and C. A. Power. 2000. International union of pharmacology: XXII. Nomenclature for chemokine receptors. *Pharmacol. Rev.* 52: 145–176.
31. Vremec, D., J. Pooley, H. Hochrein, L. Wu, and K. Shortman. 2000. CD4 and CD8 expression by dendritic cell subtypes in mouse thymus and spleen. *J. Immunol.* 164: 2978–2986.
32. Ladi, E., T. A. Schwickert, T. Chtanova, Y. Chen, P. Herzmark, X. Yin, H. Aaron, S. W. Chan, M. Lipp, B. Roysam, and E. A. Robey. 2008. Thymocyte-dendritic cell interactions near sources of CCR7 ligands in the thymic cortex. *J. Immunol.* 181: 7014–7023.
33. McCaughtry, T. M., T. A. Baldwin, M. S. Wilken, and K. A. Hogquist. 2008. Clonal deletion of thymocytes can occur in the cortex with no involvement of the medulla. *J. Exp. Med.* 205: 2575–2584.
34. Sawanobori, Y., S. Ueha, M. Kurachi, T. Shimaoka, J. E. Talmadge, J. Abe, Y. Shono, M. Kitabatake, K. Kakimi, N. Mukaida, and K. Matsushima. 2008. Chemokine-mediated rapid turnover of myeloid-derived suppressor cells in tumor-bearing mice. *Blood* 111: 5457–5466.
35. Tsou, C. L., W. Peters, Y. Si, S. Slaymaker, A. M. Aslanian, S. P. Weisberg, M. Mack, and I. F. Charo. 2007. Critical roles for CCR2 and MCP-3 in monocyte mobilization from bone marrow and recruitment to inflammatory sites. *J. Clin. Invest.* 117: 902–909.
36. Mori, K., M. Itoi, N. Tsukamoto, H. Kubo, and T. Amagai. 2007. The perivascular space as a path of hematopoietic progenitor cells and mature T cells between the blood circulation and the thymic parenchyma. *Int. Immunol.* 19: 745–753.
37. Haribhai, D., D. Engle, M. Meyer, D. Donermeyer, J. M. White, and C. B. Williams. 2003. A threshold for central T cell tolerance to an inducible serum protein. *J. Immunol.* 170: 3007–3014.
38. Quinones, M. P., S. K. Ahuja, F. Jimenez, J. Schaefer, E. Garavito, A. Rao, G. Chenaux, R. L. Reddick, W. A. Kuziel, and S. S. Ahuja. 2004. Experimental arthritis in CC chemokine receptor 2-null mice closely mimics severe human rheumatoid arthritis. *J. Clin. Invest.* 113: 856–866.
39. Lauritzsen, G. F., P. O. Hofgaard, K. Schenck, and B. Bogen. 1998. Clonal deletion of thymocytes as a tumor escape mechanism. *Int. J. Cancer* 78: 216–222.
40. Paessens, L. C., D. M. Fluitsma, and Y. van Kooyk. 2008. Haematopoietic antigen-presenting cells in the human thymic cortex: evidence for a role in selection and removal of apoptotic thymocytes. *J. Pathol.* 214: 96–103.

Supplemental Materials

Figure S1. Thymic architecture of WT and CCR2$^{-/-}$ mice. HE staining and double-color fluorescent immunostaining for CD4 (green) and CD8 (red), or Ly51 (green) and I-A^{d} (red) in WT (upper panels) and CCR2$^{-/-}$ thymus (lower panels). Representative results from three independent animals are shown. Scale bars, 200 μm.

Figure S2. Thymocyte deletion occurs independently of antigen presentation. Fifty μg anti-CD3ε mAb in PBS was injected into peritoneal cavity of DO11.10 transgenic and DO11.10/CCR2$^{-/-}$ mice. PBS was injected as a control. Two days after injection, each developmental stage of DO11.10 transgenic TCR expressing thymocytes was analyzed by FCM. Percentage and numbers of DP stage of development are shown below each panel. Representative results from three independent experiments are shown here.

Figure S3. Uptake of bloodstream mouse serum IgG by thymic Sirpα^{+} DCs. Alexa Fluor 647-conjugated mouse serum IgG (200 μg) was injected into the tail vein. PBS was injected as a control. Uptake of mouse serum IgG was analyzed 1 hr after the injection. Percentage of Sirpα (+) IgG (+) region is shown in each panel. Representative results from three independent experiments are shown here.

Figure S4. CD11c^{+}Sirpα^{+}B220^{-} cells in peripheral blood, bone marrow, and bone marrow-derived DC population. DCs were differentiated from PBMCs and bone marrow cells isolated from WT mice. The resultant DCs were stained with anti-CD11c, anti-Sirpα, and anti-B220 mAbs. The expression of Sirpα and B220 was analyzed by FCM on CD11c^{+} cells in R1 region. Percentage of differentiated CD11c^{+} bone marrow-derived DCs is shown in the lower left histogram. Representative results from

three independent animals are shown here.

Figure S5. Expression of CCR2 on CD11c^{+}Sirpα^{+} immature DCs. DCs were differentiated from PBMCs and bone marrow cells isolated from WT mice. The resultant DCs were stained with anti-CD11c, anti-Sirpα, and anti-CCR2 mAbs. CCR2 expression was analyzed by FCM on CD11c^{high}Sirpα^{+} cDCs. Gray-filled and black-open histograms indicate the results using isotype control and anti-CCR2 antibodies, respectively. Representative results from three independent animals are shown here.

Figure S6. Presumed intrathymic mechanism of bloodstream antigen transportation by Sirpα^{+} DCs. As a reference to the illustrated image, the left panel shows the serial tissue sections to delineate MCP-2 expression and Sirpα^{+} DCs localization in relation to Col IV^{+} PVR encompassed by Ly51^{+} cortical parenchyma. The mechanism of bloodstream antigen uptake by Sirpα^{+} DCs and their migration into cortical parenchyma is illustrated in the right panel.

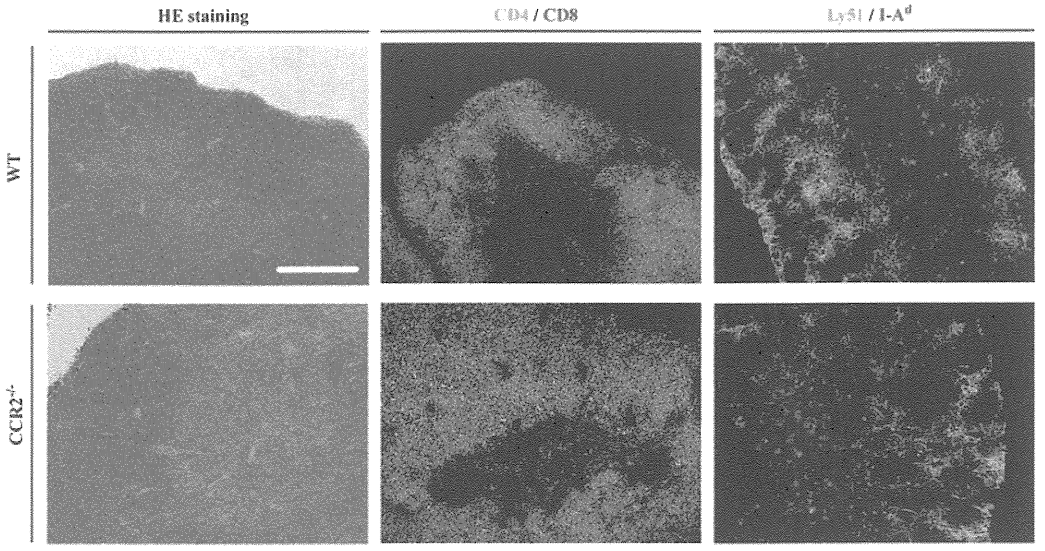

Supplementary Figure 1 Baba et al

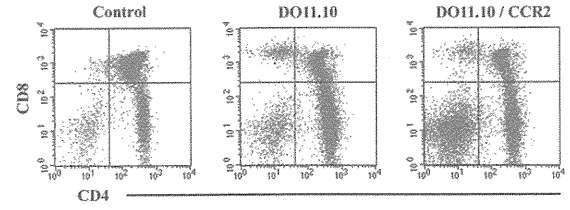

	Control	DO11.10	DO11.10 / CCR2
(%)	78.9	24.1	19.9
(x 10^7)	20.5	0.23	0.17

Supplementary Figure 2 Baba et al

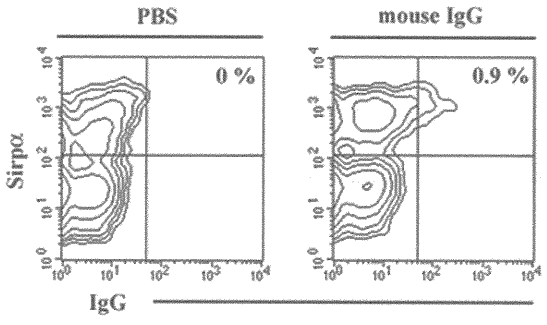

Supplementary Figure 3 Baba et al

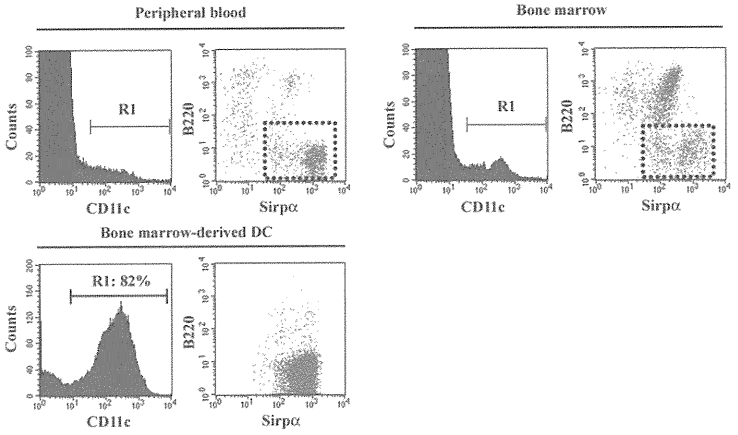

Supplementary Figure 4 Baba et al

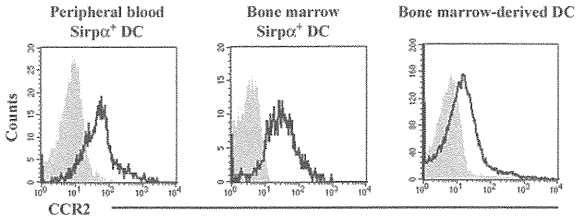

Supplementary Figure 5 Baba et al

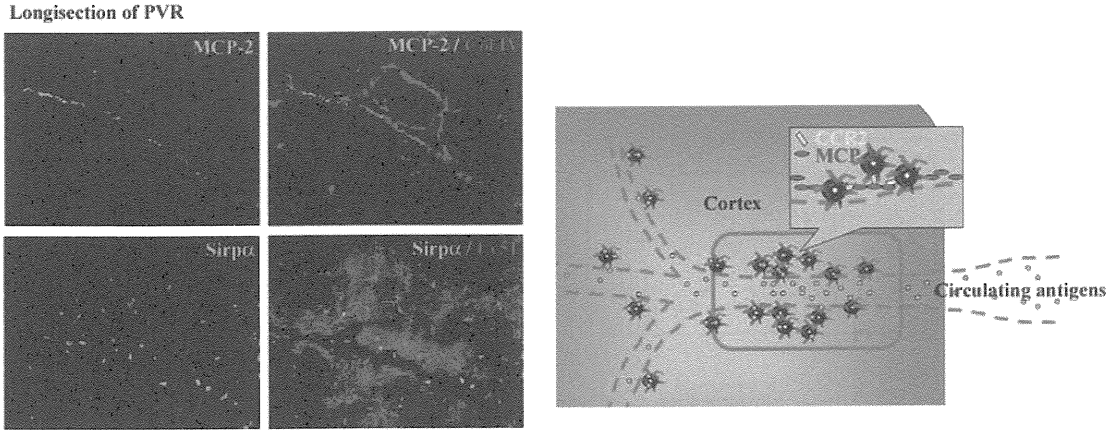

Supplementary Figure 6 Baba et al